Electronic Supplementary Material (ESI) for Materials Advances.
This journal is © The Royal Society of Chemistry 2020

Supporting Information's

Scalable solid-state synthesis of MoS_2-NiS_2/graphene nanohybrids as bifunctional electrocatalyst for enhanced overall water splitting

Sunil P. Lonkar, Vishnu V. Pillai, Saeed M. Alhassan**

Department of Chemical Engineering, Khalifa University, P.O box 127788, Abu Dhabi, UAE

E-mail: saeed.alkhazraji@ku.ac.ae; sunil.lonkar@ku.ac.ae

Tel:+971-26075944, Fax: +971-26075200

Synthesis of Graphite Oxide (GO)

Graphite oxide was prepared from natural graphite by using improved synthesis proposed by Tour *et al.* [1]. In brief, mixture of concentrated sulfuric acid (270 ml) and phosphoric acid (33 ml) was added to a 5 l *Erlenmeyer flask* placed in an ice-bath. About 5 g of natural flake graphite (10 mesh) was dispersed in the cold sulfuric acid with an overhead stirrer. Subsequently, 2.7 g of $KMnO_4$ was added slowly over 1520 min, and the resulting one-pot mixture was stirred for 72 h at room temperature to allow the oxidation of graphite. The color of the mixture changed from dark purple-green to dark brown. Later, about 35% hydrogen peroxide (H_2O_2) solution was added to terminate the oxidation process and the color of the mixture changed to bright yellow, indicating a high oxidation level of graphite. As-synthesized graphite oxide was suspended in water containing 1 M dilute hydrochloric acid to obtain a yellow-brown dispersion, which was subjected to the repeated washing with de-ionized water until a pH of 4-5 was achieved. To ensure complete removal of the residual salts and acids, dialysis process was used.

Materials Characterizations

As prepared samples of MoS_2-NiS_2/G nanohybrids and respective nanoparticles were extensively characterized using different techniques. The X-ray powder diffraction (PXRD) analyses were conducted on a Philips X'Pert Pro X-Ray diffractometer equipped with a scintillation counter and Cu-Kα radiation reflection mode. The microscopic morphology and structures of the samples were characterized using a FEI Tecnai (G20) transmission electron microscope (TEM) and FEI Titan (300 kV) high resolution transmission electron microscope (HRTEM) and Zeiss (1540 XB) scanning electron microscope (SEM) coupled with energy dispersive X-ray analysis (EDX). The X-ray photoelectron spectra (XPS) were conducted by using a Surface Science Laboratories, Inc. (SSX-100) system equipped with a monochromated Al K_α X-ray source, a hemispherical sector analyser (HSA) and a resistive anode detector. The specific surface area and porosity of the resulting MN nanohybrids were obtained using ASPS 2010 (Micromeritics, USA) Brunauer-Emmett-Teller (BET) nitrogen adsorption-desorption at liquid N_2 temperature. The samples were pre-treated at 100 ^oC in a high vacuum for 24 h before N_2 adsorption using a Quantachrome Autosorb gas-sorption system. The Raman spectra of the MN nanohybrids were measured using a Raman microscope (LabRam HR, Horiba Scientific) with an excitation wavelength of 633 nm. TGA analysis was carried out on Discovery TGA (TA instruments) using the temperature range from 30 to 900 ^oC at a ramp rate of 10 ^oC in an air atmosphere (50 mL min^{-1}). The TGA coupled mass spectroscopy was performed on Netzsch (TG 449 F3 Jupiter) STA with QMS 403 D Aeolos attachment. The ball milling performed on IKA ULTRA-TURRAX® Tube Drive control homogenizer using five stainless steel balls, each weighing 509.3 mg.

Electrochemical Measurements

The HER and OER performance of the resulting nanostructured electrocatalysts were tested using a Biologic VP300 electrochemical workstation. The standard electrochemical cell (three-electrode) configured with reference electrode [saturated calomel electrode (SCE)] and platinum wire (counter electrode), respectively was employed. The working electrodes were fabricated from as synthesized MoS_2-NiS_2/G nanohybrids by mixing it with Nafion binder in the ratio of 90:10 wt-%. The resultant homogeneous mixture was uniformly casted on a graphite foil and dried under vacuum to remove the solvent. The loading of the electrocatalsyst active materials on the both cathode and anode was retained the same i.e 0.8 ± 0.1 mg/cm^2. The measurements were performed in 0.5 M H_2SO_4 (aq) electrolyte and 1M NaOH (aq) electrolyte, respectively, both were constantly purged with Ar gas with high purity before analysis. The polarization curves were measured at 5 mV s^{-1} at ambient conditions and were compensated with iR-correction. All the potential was converted to reversible hydrogen electrode (RHE) as per following equation:

$$\boldsymbol{E_{\mathrm{RHE}} = E_{\mathrm{SCE}} + 0.059\mathrm{pH} + E^0_{\mathrm{SCE}}}$$

where the E_{RHE} is the converted potential vs. RHE, E_{SCE} is the applied potential vs. Hg/Hg_2Cl_2 SCE reference electrode, and E^0_{SCE} is the standard potential of SCE electrode at 25 °C (0.241 V). For HER, overpotential (η) = 0 V - E_{RHE}. For OER, overpotential (η) = E_{RHE} - 1.23 V. Nyquist plots were performed in the frequency range of 0.1 to 10^5 Hz with AC voltage amplitude of 10 mV. A long-term durability test was carried out using galvanostatic techniques such as chronoamperometry and chronopotnetiometry methods. All the samples were cycled at 20 mV s^{-1} until the stability of cyclic voltammetry (CV) was achieved, then the data were collected for HER and OER.

The Electrochemically active surface areas (ECSA) was calculated through performing the capacitive current associated with double-layer charging from the scan-rate dependence of CV. The CV of all samples was conducted with different scan rate in non-faradic potential window (Fig. S8). The double-layer capacitances (C_{dl}) of the samples were estimated by plotting the $\Delta J = J_a - J_c$ against the CV scan rate (Vb), where the slope was twice of C_{dl} and can be used to represent the ECSA [2].

$$C_{dl} = (\Delta j) / 2dVb$$

The ECSA can be calculated from the C_{dl} according to:

$$ECSA = C_{dl}/C_s$$

Where C_s is the specific capacitance of a flat surface with 1 cm^2 of real surface area.

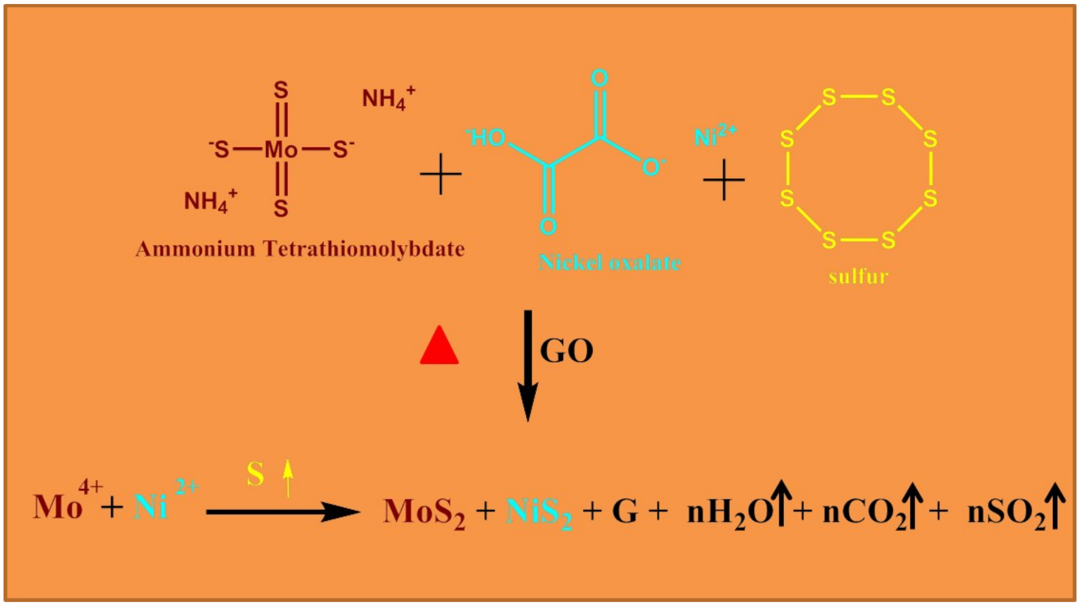

Scheme S1. Schematic representation of in-situ formation of MoS_2-NiS_2/G nanohybrid

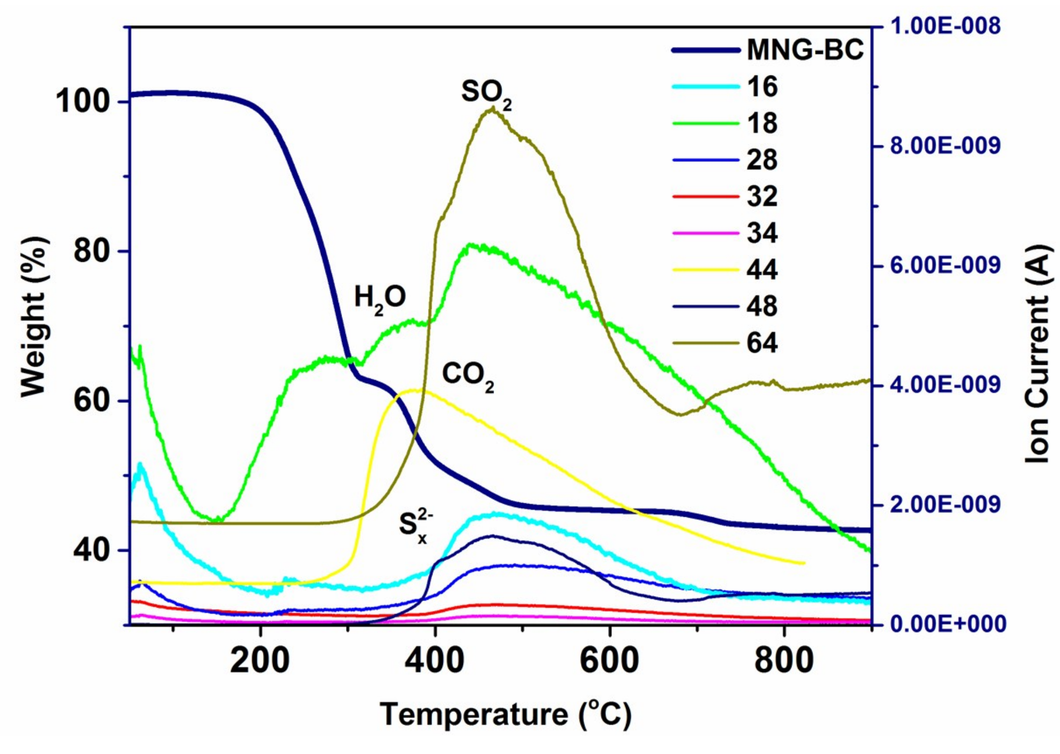

Fig.S1 TGA-MS spectra of Mo:Ni:GO precursor mix before thermal treatment

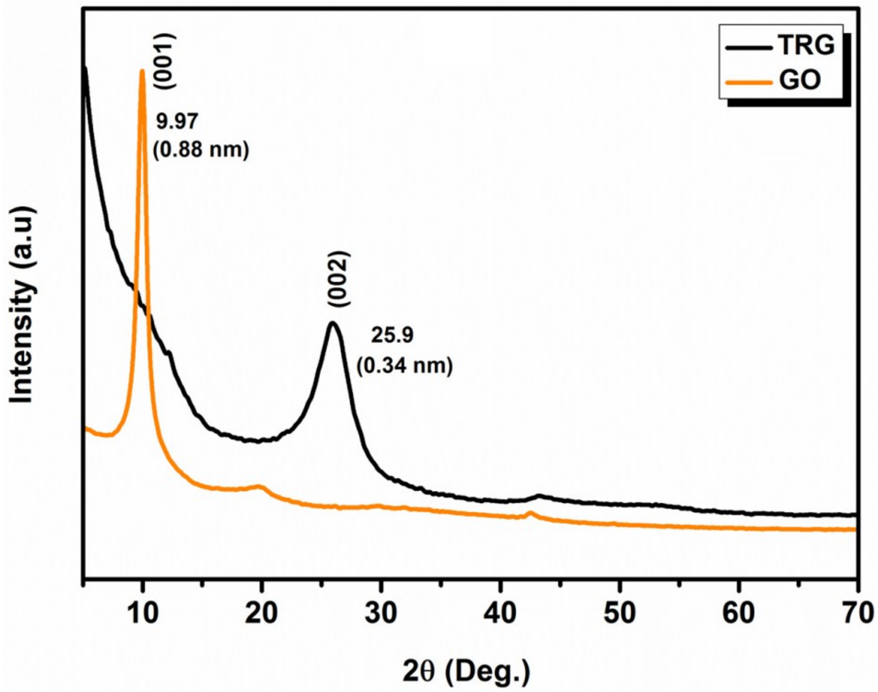

Fig. S2. XRD patterns of graphite oxide (GO) and thermally reduced graphite oxide (TRG)

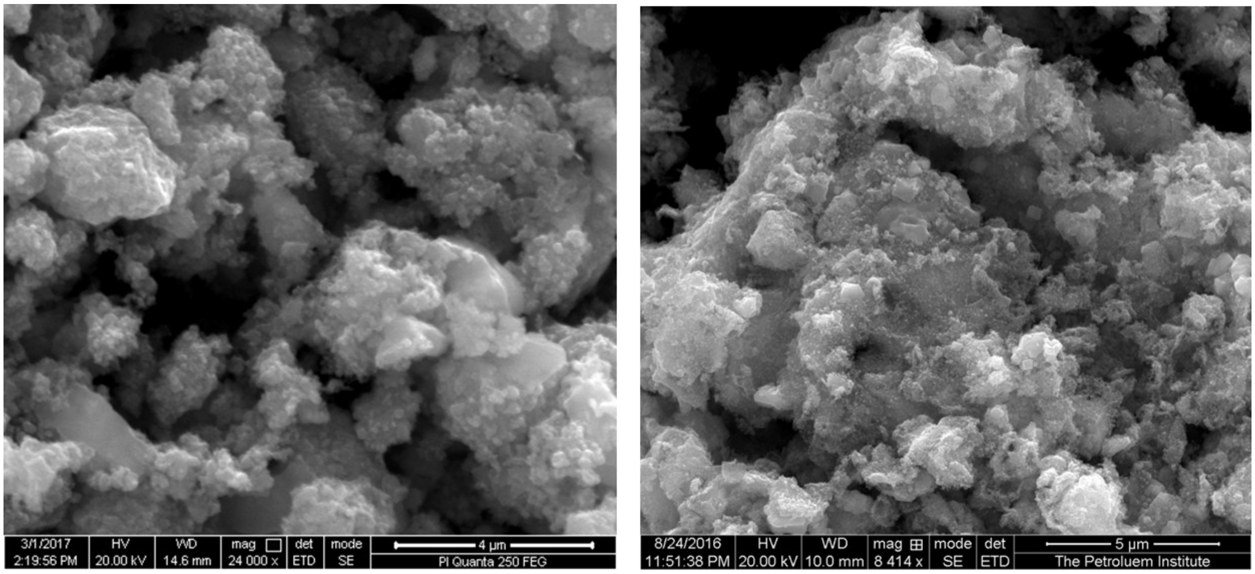

Fig.S3. SEM images of pristine MoS_2-NiS_2 nanohybrids

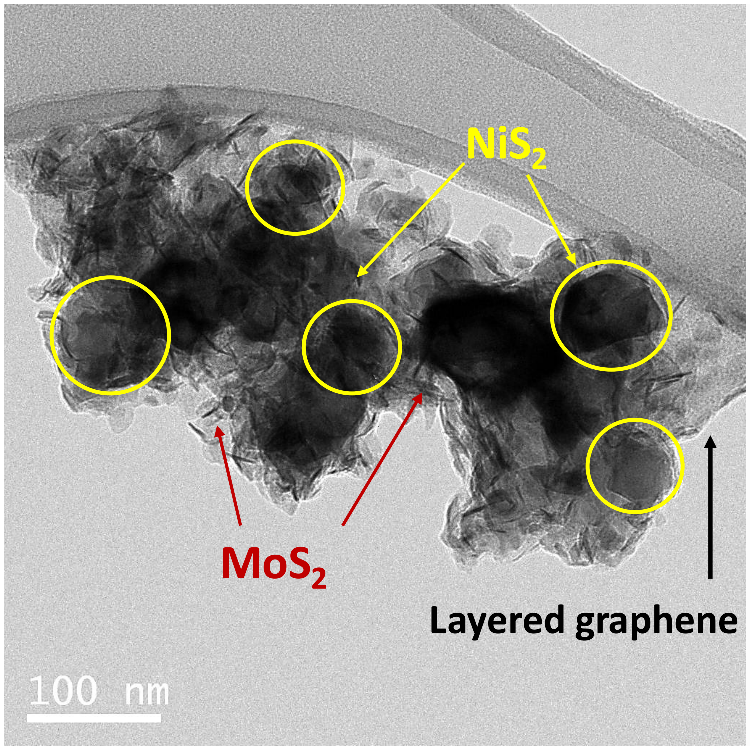

Fig.S4 TEM image of MoS_2-NiS_2/graphene nanohybrids

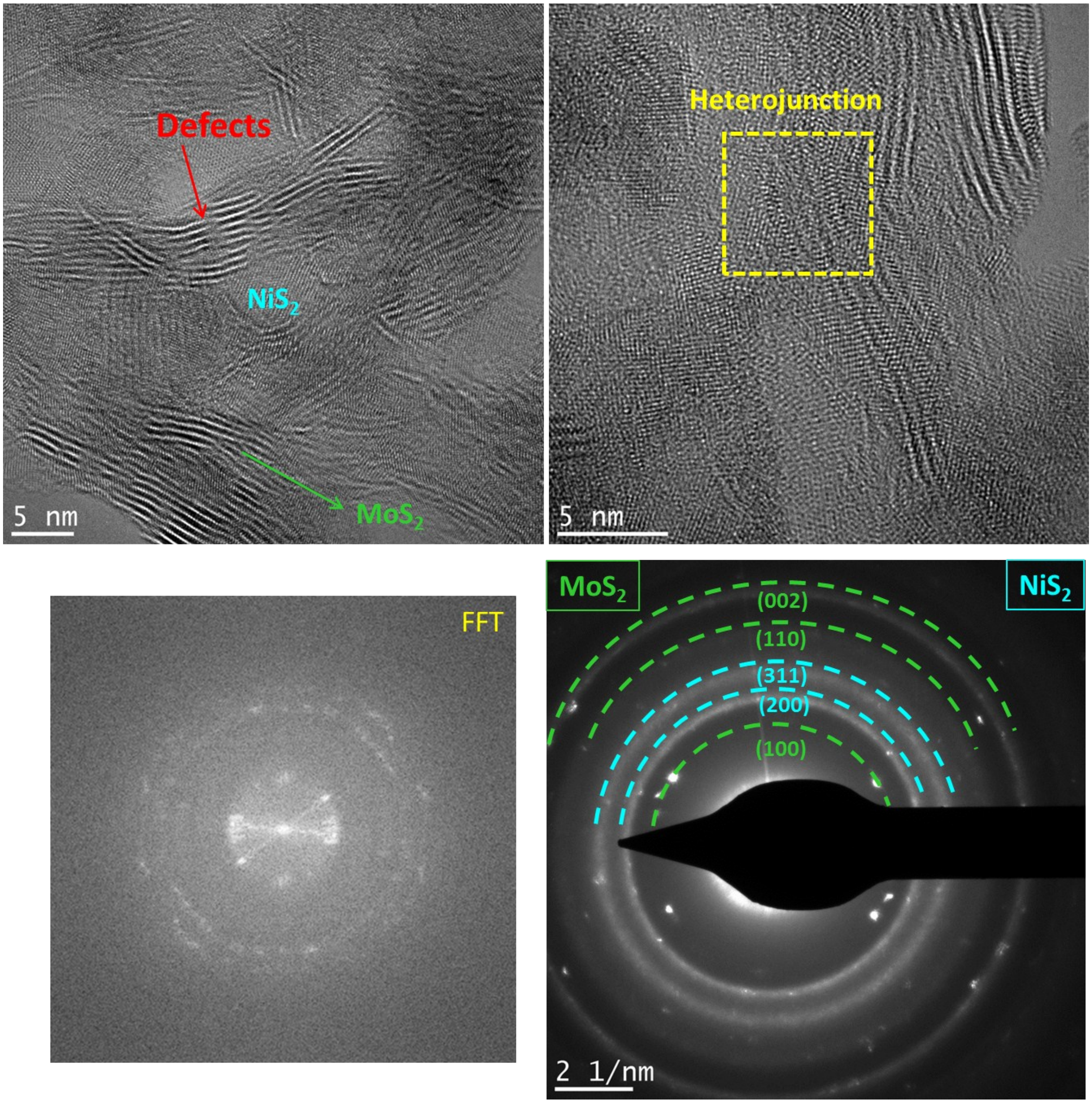

Fig.S5 The HRTEM images, FFT and SAED pattern of MoS$_2$-NiS$_2$/G nanohybrid

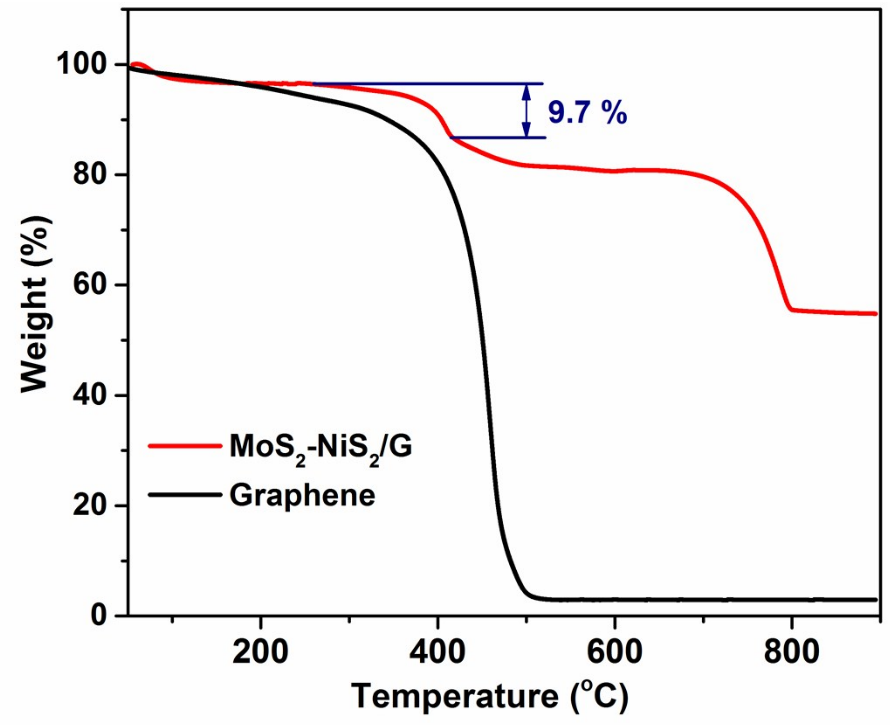

Fig.S6 TGA curves of MoS_2-NiS_2/G and thermally reduced graphite oxide (Graphene) in air.

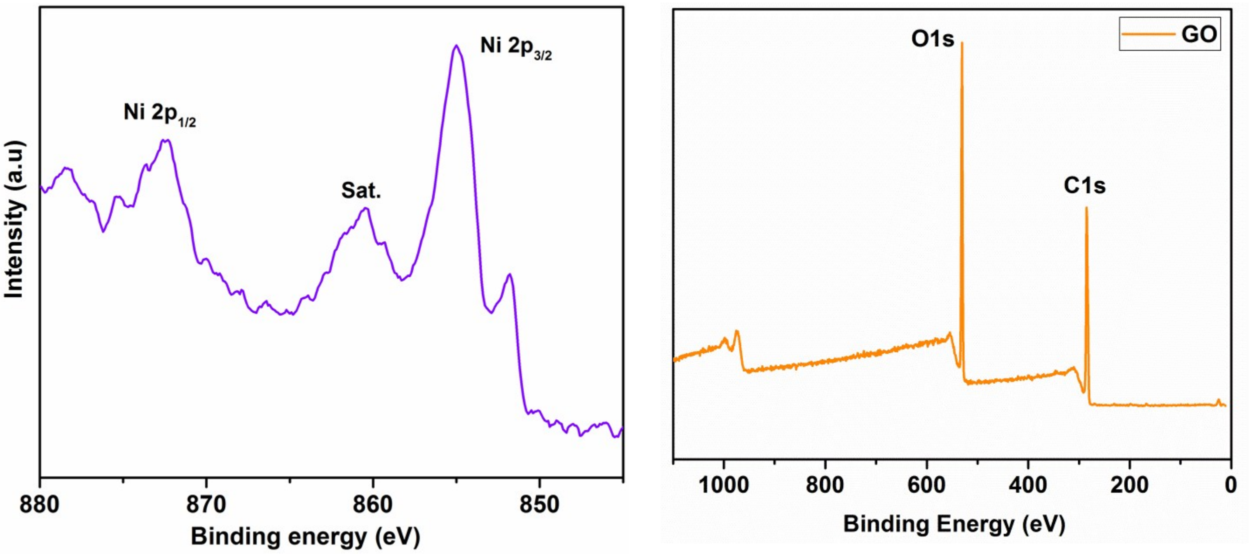

Fig. S7 High resolution XPS spectra of pristine NiS_2 and survey spectrum of GO

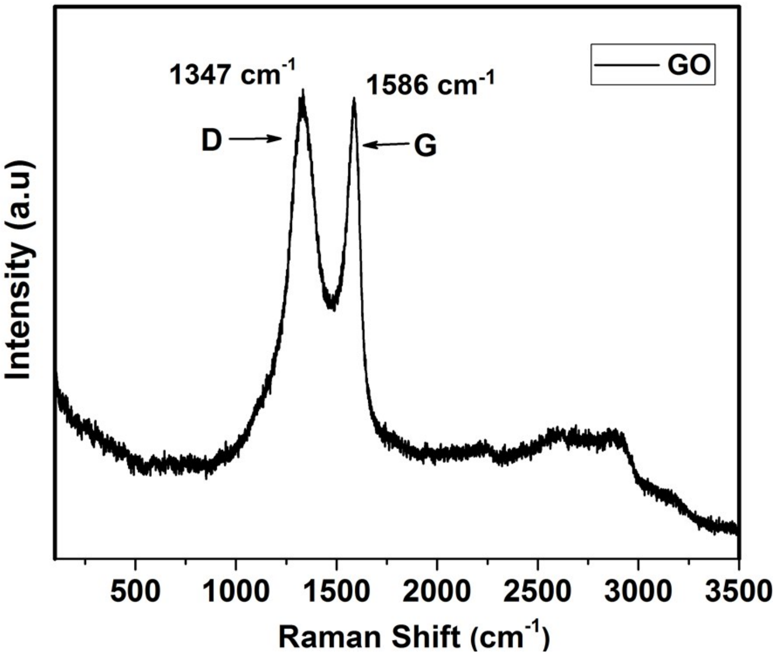

Figure S8. Raman spectra of graphene oxide.

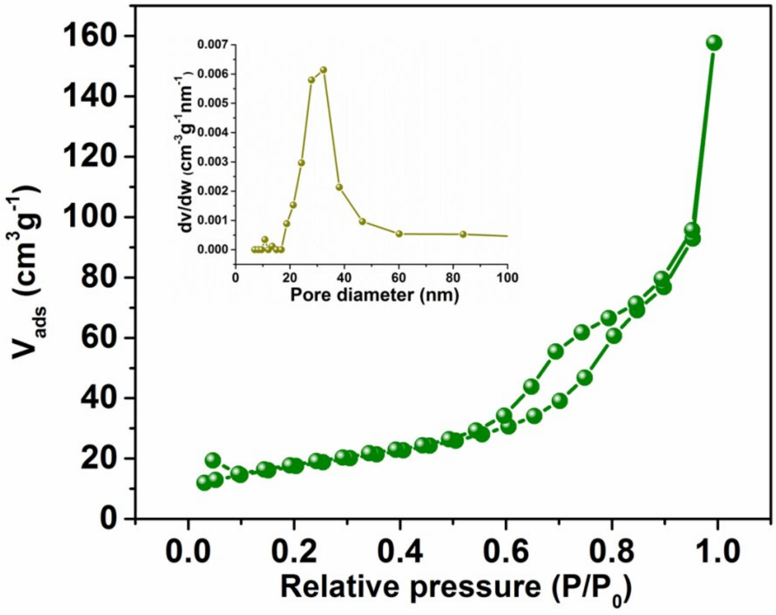

Fig. S9 N_2 adsorption-desorption isotherm of MoS_2-NiS_2 (inset-pores size distribution)

HER Mechanism in HER in both acidic and alkaline medium:

In the present study, the HER in acidic medium follows Volmer–Heyrovsky model which involves a two-electron transfer reaction, in which active catalysts are required to reduce the energy barriers in each step. The HER mechanism in acidic electrolytes is generally recognized as a combination of following three elementary steps:

(1) the Volmer step, described as hydronium (H_3O^+) discharge and formation of an adsorbed intermediate $H_{ad}^{\bullet}$ on the active site (•) (Tafel slope ~ 120 mV dec^{-1})

$$\mathbf{H_3O^+ + \bullet + e^- \rightarrow H_{ad}^{\bullet} + H_2O}$$

(2) Heyrovsky step (Tafel slope ~ 40 mV.dec^{-1})

$$\mathbf{H_3O^+ + H_{ad}^{\bullet} + e^- \rightarrow \bullet + H_2 + H_2O}$$

(3) Tafel step (Tafel slope ~ 30 mV dec^{-1}) [3]

$$\mathbf{2H_{ad}^{\bullet} \rightarrow 2\bullet + H_2}$$

In alkaline media, the HER mechanism is similar to that in acidic conditions except that $H_{ad}^{\bullet}$ is formed from dissociation of water ($H_2O + \bullet + e^- \rightarrow H_{ad}^{\bullet} + OH^-$), a step with kinetic rate depending on the binding energies of H_2O and OH_{ad} on the catalyst surface.[4] Thus, the kinetic of HER in alkaline electrolytes depends on both the rate of H_{ad} combination and the rate of H_2O dissociation.

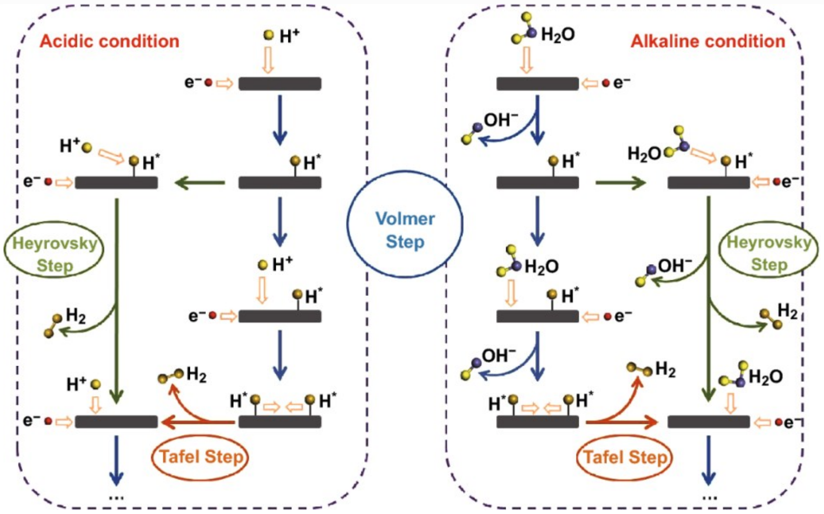

Scheme S2. Schematic pathways for hydrogen evolution reaction under acidic and alkaline conditions[5]

Calculation of active sites: The absolute number of active sites (n) for both types of MoS_2-NiS_2/G and MoS_2-NiS_2 were estimated using CV curves at a scan rate of 50 mV/s (Fig. S8). n (mol) was calculated with the equation: n=Q/(2F); where Q is the absolute voltammetry charges derived from the CV curves using equation:

$$Q = \frac{1}{Vb}\int_{E1}^{E2} IdE$$

Where, E: the potential, *Vb*: scan rate); and F is the Faraday's constant (96480 C/mol).

Table S1. Comparison of HER Activity of MoS_2-NiS_2/G nanohybrid with Other Relevant Reported Findings in 0.5 H_2SO_4 solutions

HER catalyst	**Synthesis method**	**onset potential (mV) at J $_{10\ mA/cm^2}$**	**Tafel slope (mV dec^{-1})**	**Literature**
MoS_2-NiS_2/G	Solid-State	152	53	This work
NiS_2-MoS_2/RGO	Solvothermal/Solid-Sate	172	51	[6]
MoS_2/NiS_2	Hydrothermal	235	58	[7]
MoS_2/VS_2	Hydrothermal	291	58.8	[8]
MoS_2/WS_2	Hydrothermal	167	67	[9]
MoS_2/CNTs	Spray pyrolysis	168	56	[10]
CoS_2/MoS_2	Hydrothermal	154	61	[11]
NiS2/RGO	Hydrothermal	200	52	[12]
Co-MoS_2	Hydrothermal	220	141	[13]
Ni-MoS_2/NF	Electrodeposition	207	65	[14]
20% Pt/C	Commercial Noble metal catalyst	34	30	[15]

G-Graphene, NF-Nickel foam, CC-carbon cloth

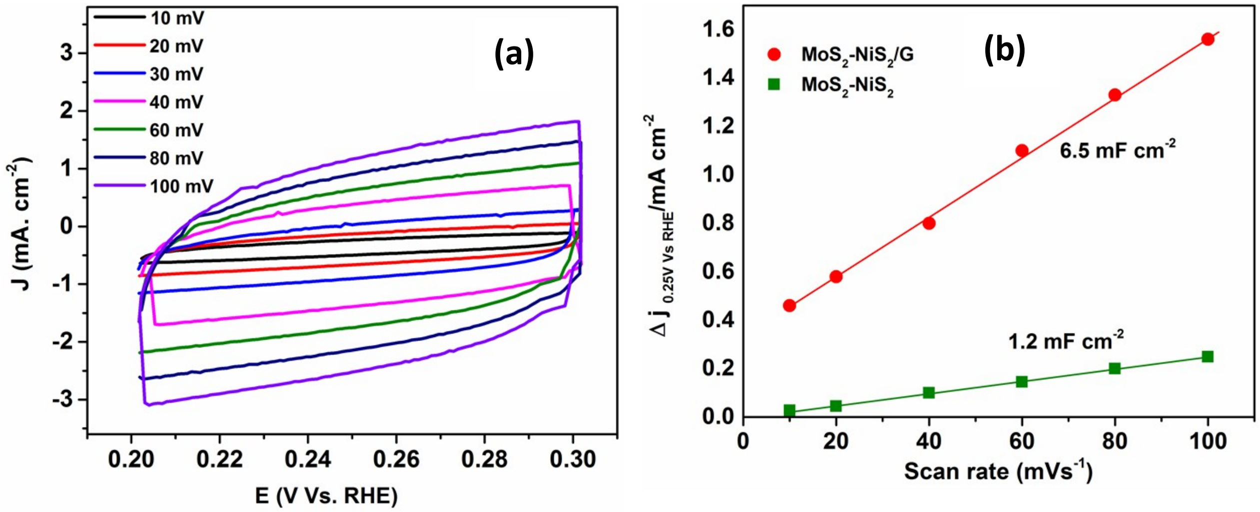

Fig.S10 (a) Cyclic voltammetry curves of MoS_2-NiS_2/G at scan rates (V_b) from 10 to 100 mV·s^{-1} and scan rate dependence of the current densities of b)

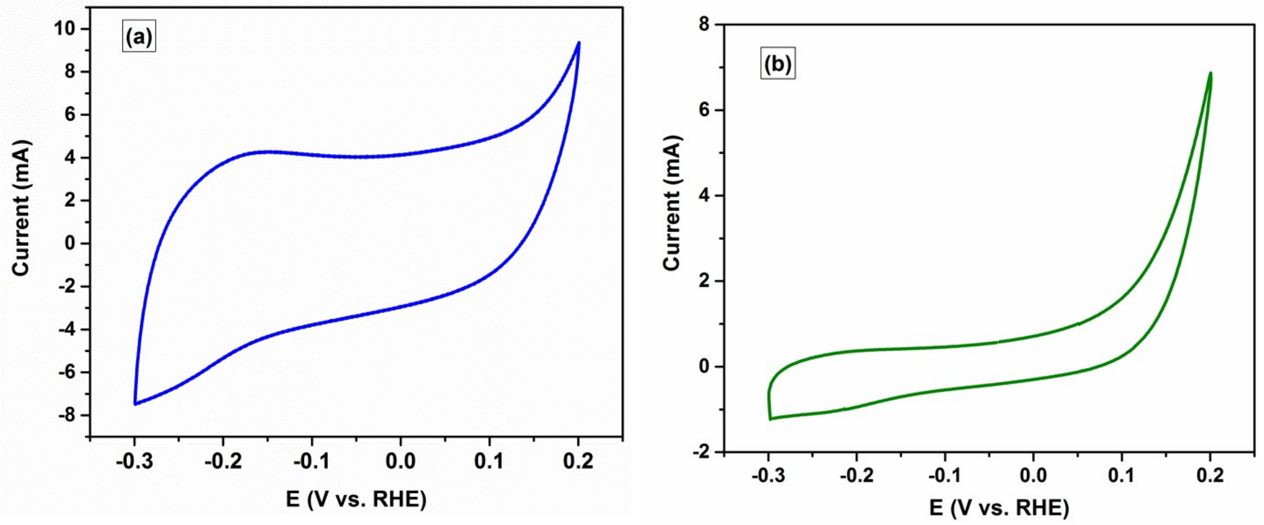

Fig.S11 Cyclic voltammetry curves of (a) MoS_2-NiS_2/G and (b) MoS_2-NiS_2 in 0.5 M H_2SO_4 vs. RHE at a scan rate of 50 mV/s.

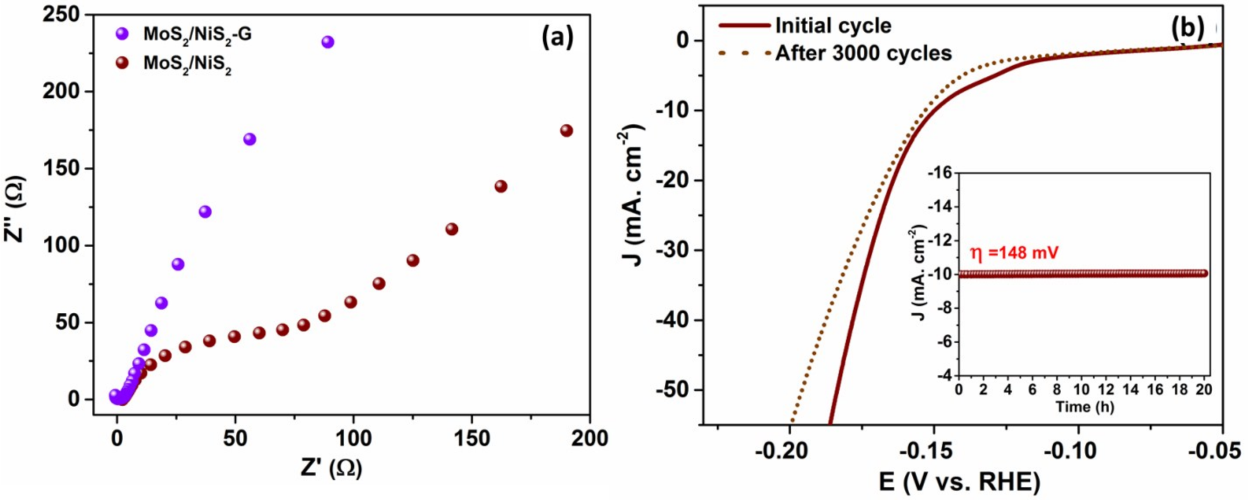

Fig.S12 a) EIS curves for MoS_2-NiS_2/G and MoS_2-NiS_2 and b) polarization curve before and after 3000 CV cycles (inset- Chronopotentiometric curve of HER) for MoS_2-NiS_2/G

Table S2. Comparison of HER Activity of MoS_2-NiS_2/G nanohybrid with Other Relevant Reported Findings in 1M KOH solution.

HER catalyst	**Synthesis method**	**onset potential (mV) at $J_{10\ mA/cm^2}$**	**Tafel slope (mV dec^{-1})**	**Literature**
MoS_2-NiS_2/G	Solid-State	141 mV	77	This work
MoS_2-NiS_2/N doped graphene	CVD	172	70	[16]
NiS-MoS_2/RGO	Solvothermal	210	65	[17]
NiS_2-MoS_2	CVD	160	70	[18]
NiS_2-MoS_2/RGO	Solvothermal/Solid-Sate	144	82	[6]
MoS_2-NiS_2	Hydrothermal	204	65	[7]
NiS_2/CoS_2/C	Co-precipitation	165	72	[19]
CoS_x/Ni_3S_2@NF	Hydrothermal	204	113	[20]
MoS_2-Ni_3S_2/NF	Solvothermal	110	83	[21]
MoS_2-NiS	Ionic liquid/Hydrothermal	244	97	[22]

G-Graphene, NF-Nickel foam, CC-Carbon cloth

Table S3. Comparison of OER Activity of MoS_2-NiS_2/G nanohybrid with Other Relevant Reported Findings in alkaline solutions

HER catalyst	**Synthesis method**	**onset potential (mV) at $J_{10\ mA/cm^2}$**	**Tafel slope (mV dec^{-1})**	**Literature**
MoS_2-NiS_2/G	Solid-State	320	82	This work
MoS_2-NiS_2/N doped graphene	CVD	370	70	[16]
MoS_2-Ni_3S_2	Hydrothermal	349	87	[23]
NiS-MoS_2/CC	Hydrothermal	333	77	[24]
MoS_2-NiS	Solvothermal/surfactants	371	74	[25]
Co-MoS_2	Hydrothermal	390	177	[13]

G-Graphene, NF-Nickel foam, CC-carbon cloth

References

1. D. C. Marcano, D. V. Kosynkin, J. M. Berlin, A. Sinitskii, Z. Z. Sun, A. Slesarev, L. B. Alemany, W. Lu and J. M. Tour, *Acs Nano*, 2010, **4**, 4806-4814.
2. Y. Lin, J. Zhang, Y. Pan and Y. Liu, *Appl. Surf. Sci.*, 2017, **422**, 828-837.
3. V. R. Stamenkovic, D. Strmcnik, P. P. Lopes and N. M. Markovic, *Nature Materials*, 2017, **16**, 57-69.
4. R. Subbaraman, D. Tripkovic, K. C. Chang, D. Strmcnik, A. P. Paulikas, P. Hirunsit, M. Chan, J. Greeley, V. Stamenkovic and N. M. Markovic, *Nature Materials*, 2012, **11**, 550-557.
5. J. Wei, M. Zhou, A. Long, Y. Xue, H. Liao, C. Wei and Z. J. Xu, *Nano-Micro Lett*, 2018, **10**, 75.
6. L. Wang, T. Guo, S. Sun, Y. Wang, X. Chen, K. Zhang, D. Zhang, Z. Xue and X. Zhou, *Catal Lett*, 2019, **149**, 1197-1210.
7. P. Y. Kuang, T. Tong, K. Fan and J. G. Yu, *Acs Catalysis*, 2017, **7**, 6179-6187.
8. C. C. Du, D. X. Liang, M. X. Shang, J. L. Zhang, J. X. Mao, P. Liu and W. B. Song, *Acs Sustain Chem Eng*, 2018, **6**, 15471-15479.
9. S. Hussain, K. Akbar, D. Vikraman, K. Karuppasamy, H. S. Kim, S. H. Chun and J. W. Jung, *Inorg Chem Front*, 2017, **4**, 2068-2074.
10. Z. F. Ye, J. Yang, B. Li, L. Shi, H. X. Ji, L. Song and H. X. Xu, *Small*, 2017, **13**.
11. L. L. Chen, W. X. Yang, X. J. Liu and J. B. Jia, *International Journal of Hydrogen Energy*, 2017, **42**, 12246-12253.
12. R. Chen, Y. Song, Z. Wang, Y. Gao, Y. Sheng, Z. Shu, J. Zhang and X. a. Li, *Catal Commun*, 2016, **85**, 26-29.
13. C. R. Wang, S. Wang, J. G. Lv, Y. X. Ma, Y. Q. Wang, G. L. Zhou, M. S. Chen, M. Zhao, X. S. Chen and L. Yang, *Int J Electrochem Sc*, 2019, **14**, 9805-9814.

14. X. Yin, H. Dong, G. Sun, W. Yang, A. Song, Q. Du, L. Su and G. Shao, *International Journal of Hydrogen Energy*, 2017, **42**, 11262-11269.
15. M. Chen, Y. Ma, Y. Zhou, C. Liu, Y. Qin, Y. Fang, G. Guan, X. Li, Z. Zhang and T. Wang, *Catalysts*, 2018, **8**, 294.
16. P. Kuang, M. He, H. Zou, J. Yu and K. Fan, *Applied Catalysis B: Environmental*, 2019, **254**, 15-25.
17. H. Wu, Y. Qiu, J. Zhang, G. Chai, C. Lu and A. Liu, *Funct Mater Lett*, 2016, **09**, 1650058.
18. T. An, Y. Wang, J. Tang, W. Wei, X. Cui, A. M. Alenizi, L. Zhang and G. Zheng, *Journal of Materials Chemistry A*, 2016, **4**, 13439-13443.
19. W. L. Xin, W. J. Jiang, Y. J. Lian, H. Li, S. Hong, S. L. Xu, H. Yan and J. S. Hu, *Chem Commun*, 2019, **55**, 6134-6134.
20. S. Shit, S. Chhetri, W. Jang, N. C. Murmu, H. Koo, P. Samanta and T. Kuila, *ACS Applied Materials & Interfaces*, 2018, **10**, 27712-27722.
21. J. Zhang, T. Wang, D. Pohl, B. Rellinghaus, R. Dong, S. Liu, X. Zhuang and X. Feng, *Angewandte Chemie International Edition*, 2016, **55**, 6702-6707.
22. Q. Qin, L. Chen, T. Wei and X. Liu, *Small*, 2019, **15**, 1803639.
23. Y. Yang, K. Zhang, H. Lin, X. Li, H. C. Chan, L. Yang and Q. Gao, *ACS Catalysis*, 2017, **7**, 2357-2366.
24. S. Guan, X. Fu, Z. Lao, C. Jin and Z. Peng, *Sustain Energ Fuels*, 2019, **3**, 2056-2066.
25. Z. Zhai, C. Li, L. Zhang, H.-C. Wu, L. Zhang, N. Tang, W. Wang and J. Gong, *Journal of Materials Chemistry A*, 2018, **6**, 9833-9838.